Electronic Supplementary Material (ESI) for Journal of Materials Chemistry A

Supporting Information

Nearly Monodispersed $In(OH)_3$ Hierarchical Nanospheres and Nanocubes: Tunable Ligand-Assisted Synthesis and Their Conversion into Hierarchical In_2O_3 for Gas Sensing

Jiantao Zai, [a] *Jun Zhu,** [a,b] *Rongrong Qi* * [a] *and Xuefeng Qian* [a]

[a] School of Chemistry and Chemical Engineering and State Key Laboratory of Metal Matrix Composites, Shanghai Jiao Tong University, Shanghai, 200240 (P. R. China).

[b] National Engineering Research Center for Nanotechnology, 28 East Jiang Chuan Rd, Shanghai 200241(P. R. China).

Corresponding authors: Fax:(+86) 21-5474-1297; Tel: (+86) 21-5474-3262;E-mail:rrqi@sjtu.edu.cn; Tel: (+86) 21-3429-1286; Fax: (+86) 21-3429-1125, E-mail: yzjzhu@163.com.

Supporting Information 1

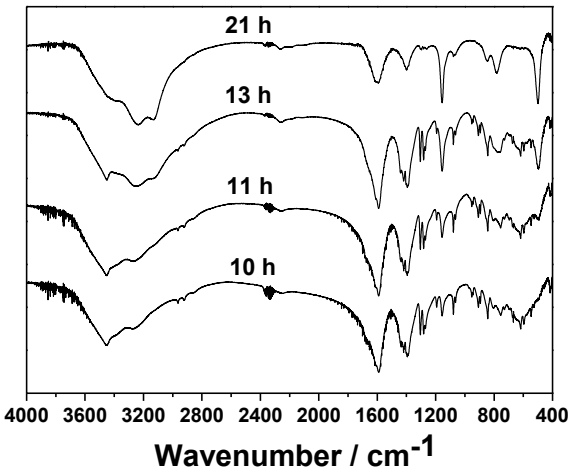

Figure S1. FT-IR spectra of $In(OH)_3$ obtained in the time-dependent experiments.

The time-evaluated FT-IR spectra of intermediate samples are shown in Figure S1. Extending the reaction time, the intensity of –OH characteristic peak between 3450 cm^{-1} decreases, and the intensity of $–NH_2$ characteristic peak at 3127 cm^{-1} increases. The characteristic peak of $–NH_2$ becomes visible at the reaction time of 13 h.

Supporting Information 2

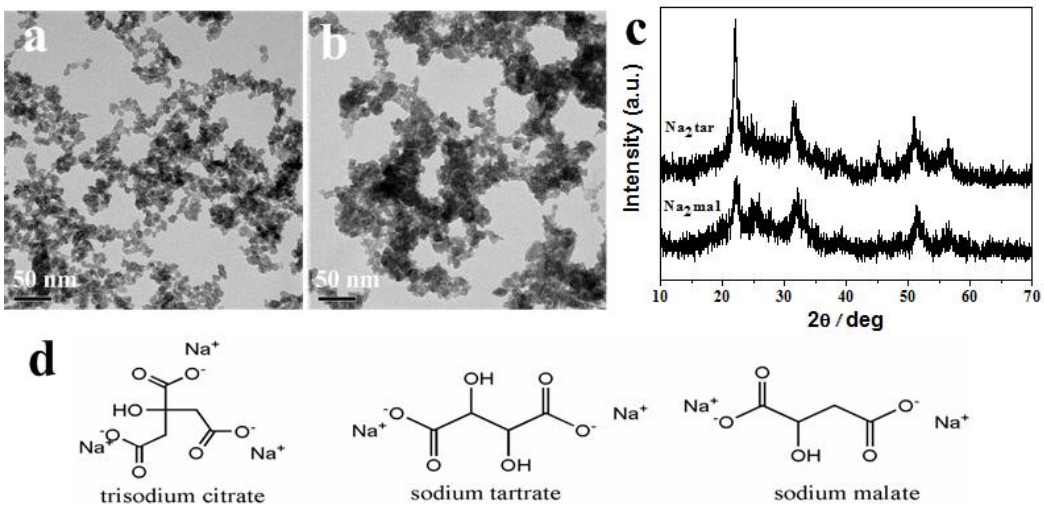

Figure S2. (a-b) TEM images and (c) XRD pattern of $In(OH)_3$ obtained at 140 ^oC, 6:1 molar ratio of Ligand/In^{3+} with different complexing agent: (a) Na_2tar, (b) Na_2mal, (d) the chemical configuration of the complexing agents.

As shown in Figure S2, it is found that irregular nanoparticles rather than well-aggregations are obtained using Na_2tar (Figure S2a) or Na_2mal (Figure S2b) as complexing agents even though the pure $In(OH)_3$ can be obtained (Figure S2c). The above results reveal that Na_2tar and Na_2mal can effectively control the crystal growth of $In(OH)_3$ nanoparticles, but hinder these nanoparticles to assemble hierarchical morphologies. The possible reasons come from the molecule structural difference between Na_3cit, Na_2tar and Na_2mal (Figure S2d). It is evident that Na_3cit has three carboxyls, while both Na_2tar molecule and Na_2mal molecule have two carboxyls. Generally, the binding of citric acid to the crystal plane proceeds through the two methylene-carboxyl groups. The carboxyl group that is shorter than the methylene-carboxyl groups does not reach the surface and remains passive but it activates all oxygen atoms of the methylene-carboxyl groups by accepting a hydrogen atom. Thus, in present system, COO^- ions of two methylene-carboxyl groups in Na_3cit molecule bind to the $In(OH)_3$ nanoparticles and the other COO- ions in Na_3cit molecule can interact with other functional groups through hydrogen bonding. However, there are no free COO- in Na_2tar molecule and Na_2mal molecule for the formation of

additional hydrogen bonding after binding with $In(OH)_3$ nanoparticles, which lead to the irregular nanoparticles instead of well-aggregations.

Supporting Information 3

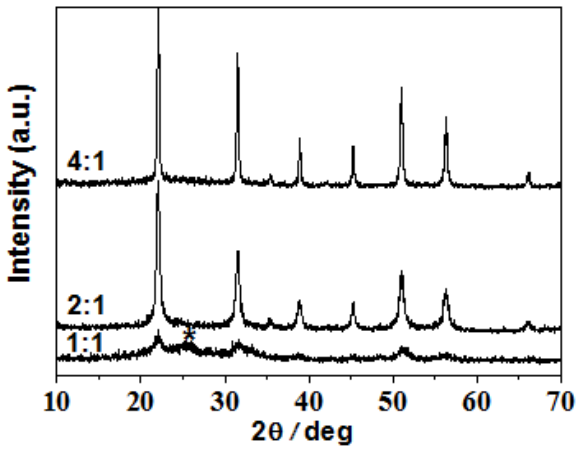

Figure S3. XRD patterns of $In(OH)_3$ obtained at 140 ^oC with different molar ratio of cit^{3-}/In^{3+}.

Supporting Information 4

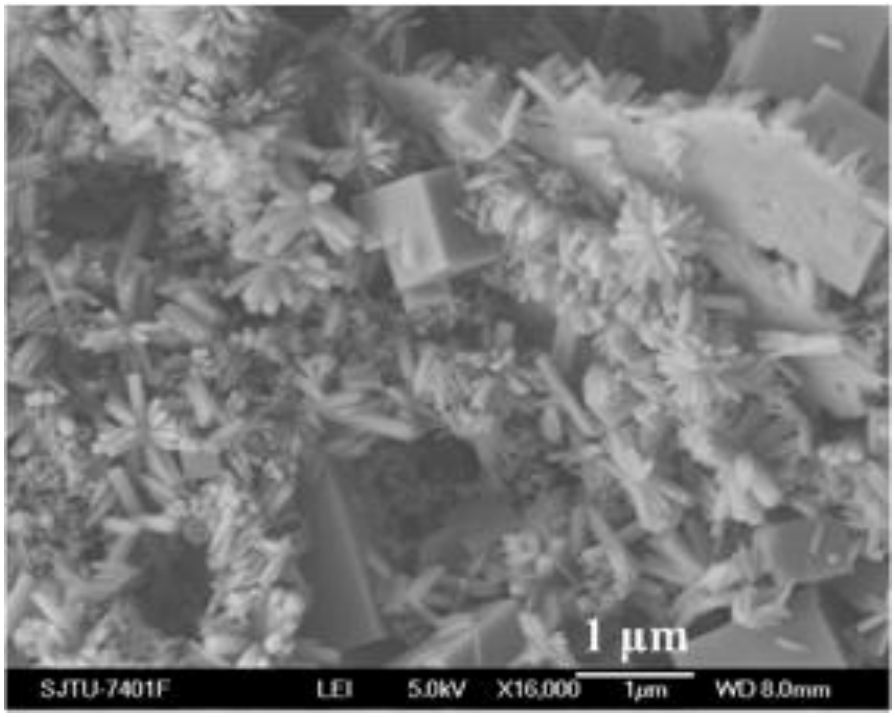

Figure S4. SEM images of $In(OH)_3$ obtained at 140 ^oC for 24 h in absence of Na_3cit.

Supporting Information 5

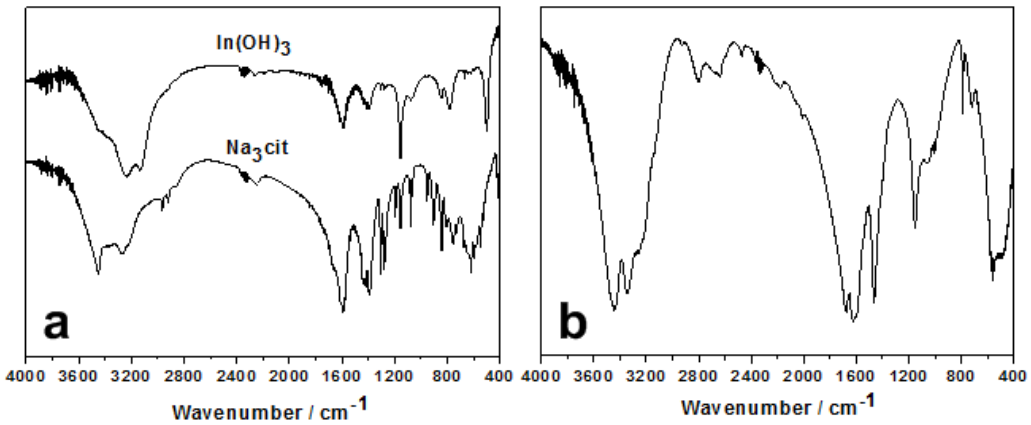

Figure S5. (a) FT-IR spectra of Na_3cit and $In(OH)_3$ obtained at 140 ^oC with 6:1 molar ratio of cit^{3-}/In^{3+} for 24 h; (b) FT-IR spectra of urea.

The FT-IR spectra of Na_3cit and $In(OH)_3$ obtained at 140 ^oC with 6:1 molar ratio of cit^{3-}/In^{3+} for 24 h are shown in Figure S5a. In the spectra of Na_3cit, two strong bands at 1592 and 1397 cm^{-1} are attributed to characteristic asymmetric and symmetric stretching vibrations of COO-, respectively. The bands between 3450 and 3260 cm^{-1} corresponds to characteristic stretching vibration of OH group. In additional, the –OH group gives the deformation vibration bands at 1290, 1210, 1089 and 1080 cm^{-1}, which are also characteristic of undissociated alcoholic –OH group. However, compared with the FT-IR spectra of urea (Figure S5b), in the spectra of $In(OH)_3$ product, two strong bands at 3242 and 3127 cm^{-1} could be found besides the strong absorption peaks at 500 cm^{-1} of $In(OH)_3$, which results from the stretching vibration of $–NH_3$. Additionally, a weak bands at about 1750 cm^{-1} (indicated by arrow) also appears, which comes from stretching vibration of –C=O group in COO-. Meanwhile, due to the formation of hydrogen bonding of –OH group in Na_3cit, the peak at 3260 cm^{-1} of –OH group in Na_3cit

disappears and the peak at 3450 cm^{-1} of –OH group in Na3cit becomes broad. These results reveals that there are many hydrogen bonding interactions among functional groups, such as –OH, -C=O, $-NH_2$ and –COO- ion and these hydrogen bonding interactions contribute to the formation of assembled $In(OH)_3$ nanostructures. In other words, both Na_3cit and NH_3 can absorb on $In(OH)_3$ nanoparticles and then contribute to the assembly of $In(OH)_3$ nanoparticles through interaction between Na_3cit and NH_3 molecules on adjacent nanoparticles.

Supporting Information 6

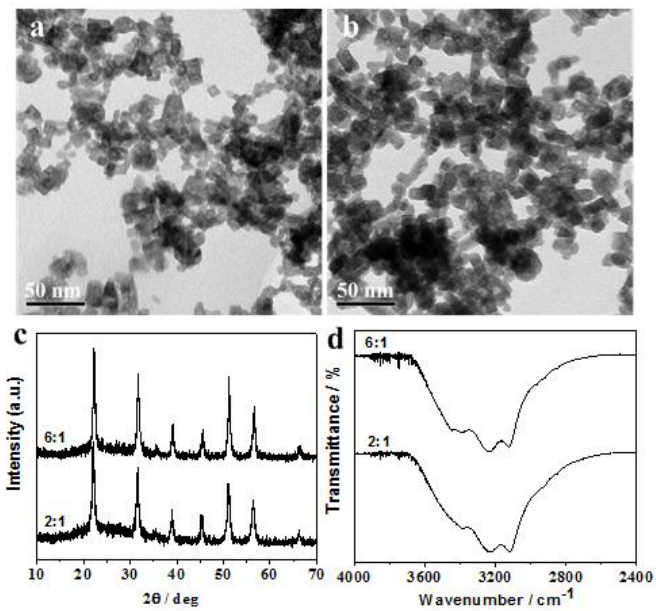

Figure S6. (a-b) TEM images, (c) XRD patterns and (d) FT-IR spectra of $In(OH)_3$ obtained at 140 ^oC, En as alkaline source with different molar ratio of cit^{3-}/In^{3+}: (a) 2:1; (b) 6:1.

Urea was replaced by En to perform at similar reaction condition. However, the obtained products are also irregular nanocubes instead of well-aggregations no matter the molar ratio of cit^{3-}/In^{3+}(Figures S6a-b) even if the samples are high purity in XRD pattern (Figure S6c). In comparison with that of urea, functional group of –C=O in urea is substituted by $–CH_2$ group in En. This goes against the hydrogen bonding, which have been proved by FT-IR spectra (Figure S6d). In the FT-IR spectra, the relative intensity of –OH peaks of Na_3cit are stronger than that in the Na_3cit/urea system, indicating most of –OH groups of Na_3cit are free from the formation of hydrogen bonding.

Supporting Information 7

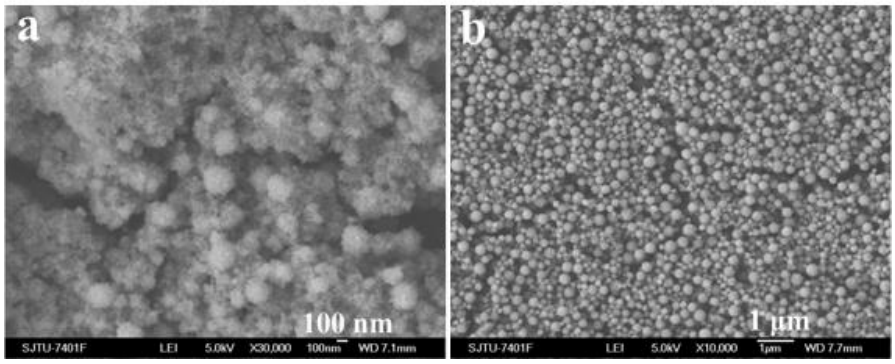

Figure S7. SEM images of $In(OH)_3$ obtained at 140 ^oC, 0.8 mmol of Na_3cit with different molar ratio of EDTA/In^{3+}: (a) 0.5 : 1; (b) 1 : 1.

In order to further explore the real factors affecting the morphologies or the self-assembled styles of $In(OH)_3$, the additional ligand including multi-group, such as EDTA, were introduced to the present system, the hierarchical $In(OH)_3$ assembly could be reformed. As shown in Figure S7, with the addition of EDTA, the morphology of $In(OH)_3$ changes from nanoparticles, to part-assembled spherical structures and to full-assembled spherical structures at the 2:1 molar ratio of cit^{3-}/In^{3+}. The reasons can be attributed to the hydrogen bonding between Na_3cit and in EDTA. Therefore, based on the above experiment results, both Na_3cit and urea contributes to the formation of hierarchically assembled $In(OH)_3$ structures inducing by hydrogen bonding interactions.

Supporting Information 8

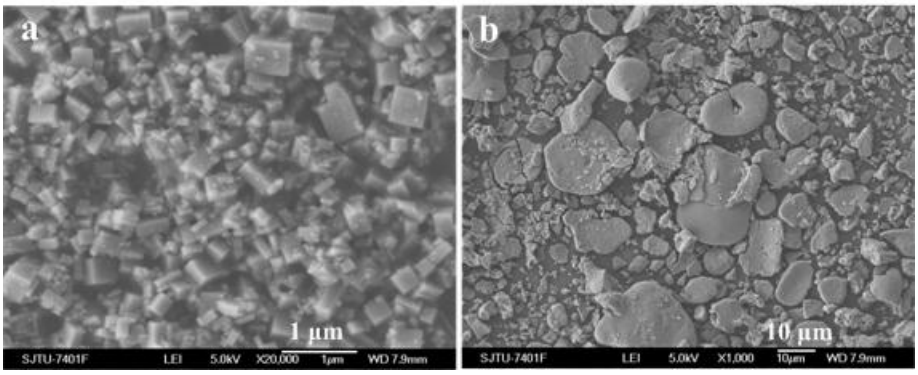

Figure S8. SEM images of $In(OH)_3$ obtained at 140 ^oC with 6:1 molar ratio of cit^{3-}/In^{3+} for 24 h with different alkaline source: (a) NaOH; (b) $NH_3 \cdot H_2O$.

Supporting Information 9

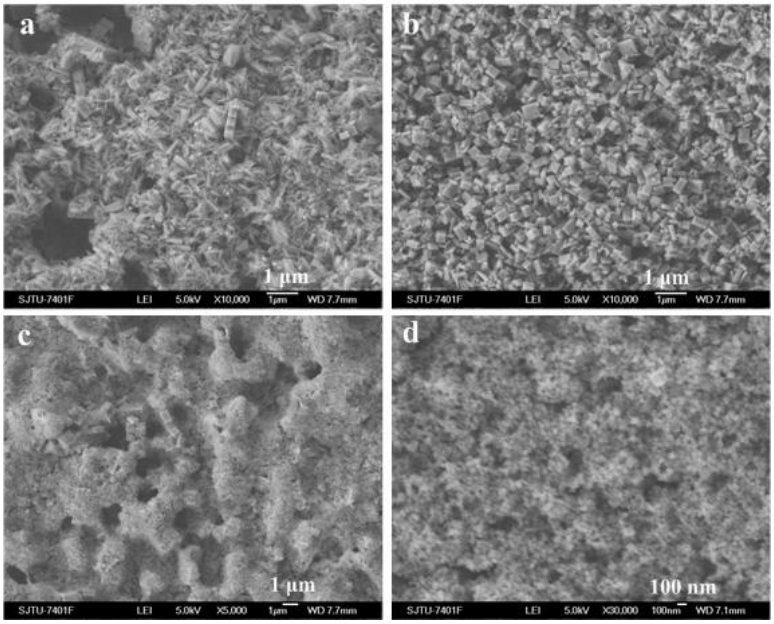

Figure S9. SEM images of $In(OH)_3$ obtained in the system of EDTA at different molar ratio of $EDTA/In^{3+}$: (a) 0.2 : 1; (b) 0.5 : 1; (c) 0.8 : 1; (d) 1 :1.

Supporting Information 10

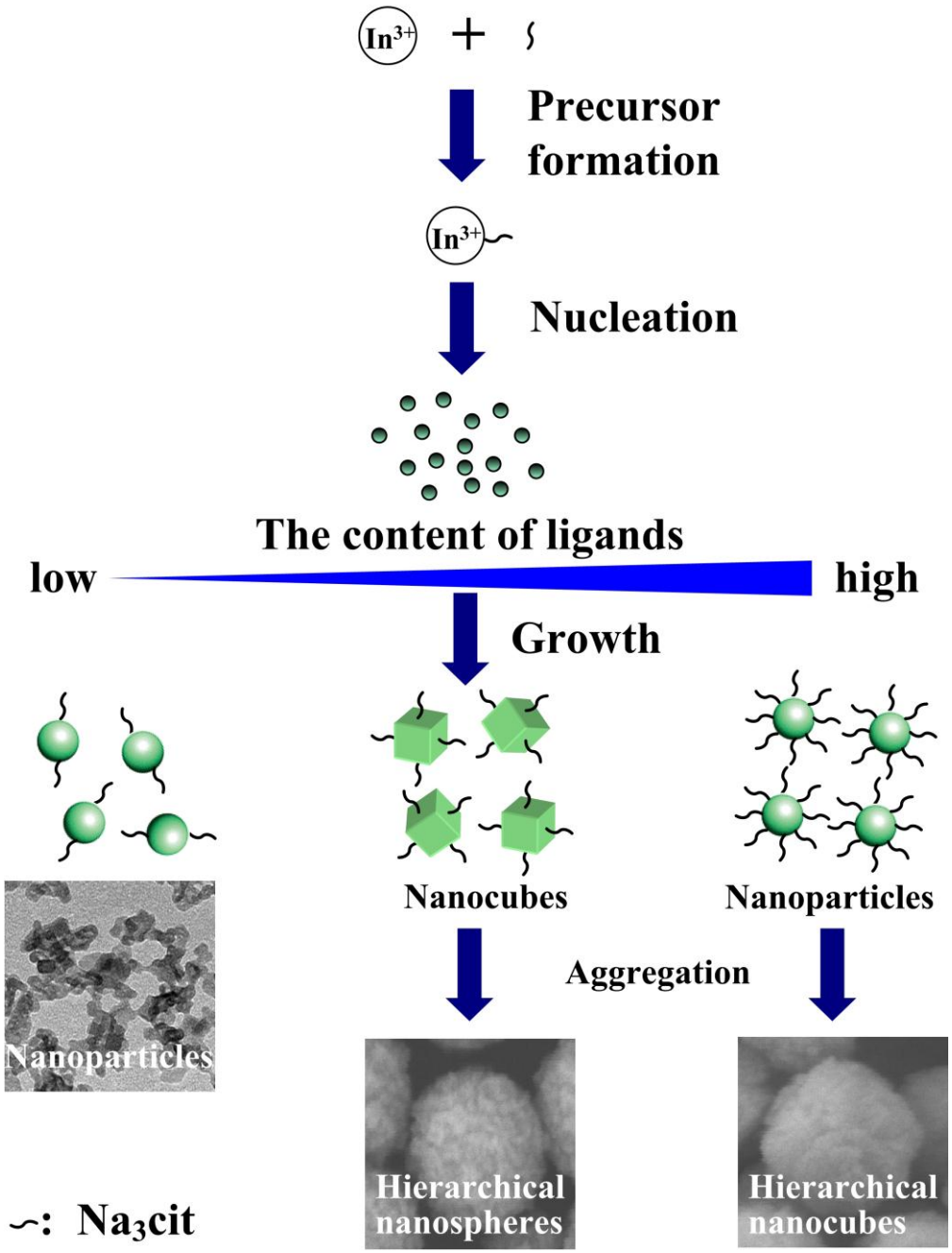

Figure S10. Schematic illustration of the formation process of $In(OH)_3$ different morphologies or hierarchical structures, such as nanoparticles, monodispersed hierarchical nanospheres and nanocubes.

From the schematic illustration of Figure S10, one can see that ligand was first complexed with In^{3+} ions to create $In(cit)_n$ complexation, which would affect the nucleation rate of $In(OH)_3$. On the other hand, the added ligand also can absorb on the surface of $In(OH)_3$ crystallites, and further affect the final morphology of the obtained products. For example, only nanoparticles were obtained because of the

incomplete capping of primary $In(OH)_3$ crystallites in the lower content of ligands; nanospheres "building blocks" were obtained because of the excess capping of primary $In(OH)_3$ crystallites in the higher content of ligands; and nanocubes "building blocks" were only obtained at suitable content of ligands, because of the co-effects of $In(OH)_3$ inherent crystal nature and the selective absorption of ligand on the facets of $In(OH)_3$.

Supporting Information 11

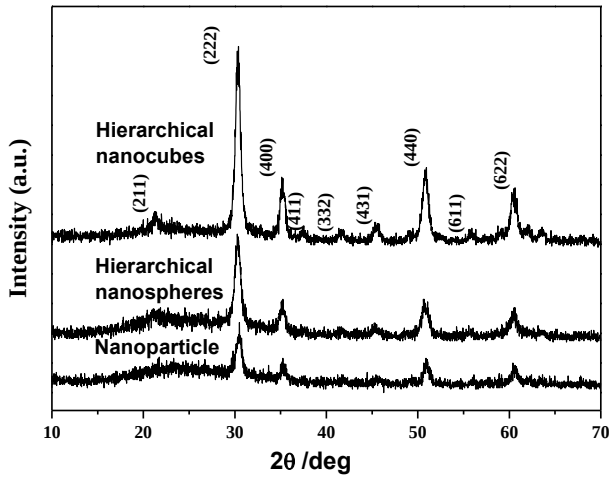

Figure S11. XRD patterns of In_2O_3 different nanostructures annealing the corresponding $In(OH)_3$ samples.

Supporting Information 12

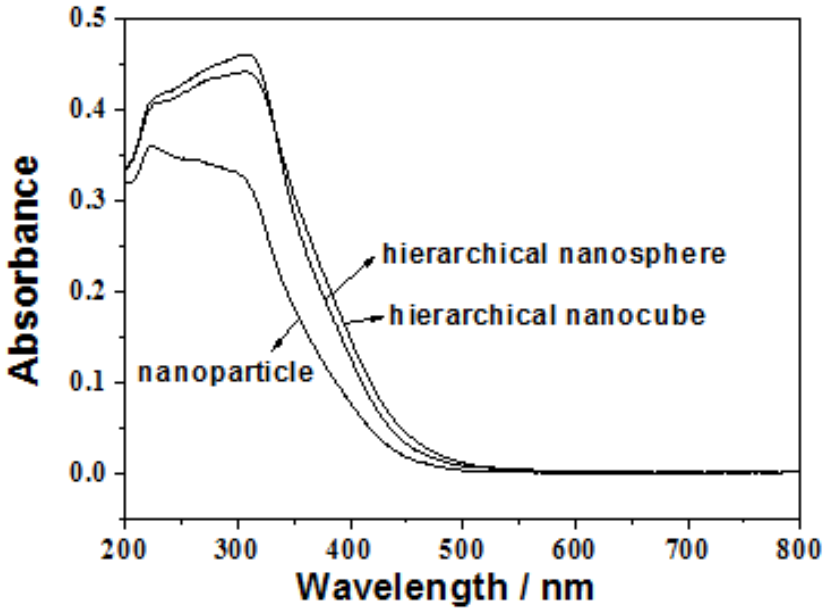

Figure S12 UV-diffuse reflectance spectrum of the In_2O_3 samples of nanoparticles, hierarchical nanosphere and hierarchical nanocube.

Diffuse reflectance spectroscopy (DRS) and its applications in studying metal oxides have been reviewed recently.[26] As a kind of n-type semiconductor with direct band gap, In_2O_3 has been widely

studied because of its potential application for solar cell combining with a suitable p-type semiconductor. The UV-diffuse reflectance spectra of the as-obtained In_2O_3 nanostructures with different morphology are shown in Fig. 7. Different from the absorption of bulk In_2O_3 at 330 nm (3.75 eV), the absorption peaks of all In_2O_3 products are among 300-310 nm. The blue-shift of absorption peaks implies that the obtained In_2O_3 particles are in nano-size and possess a weak quantum confinement effect. Compared to the absorption peak of nanoparticles at 300 nm, the absorption peaks of hierarchical In_2O_3 nanospheres and nanocubes are at about 310 nm because the scattering of light reduces the absorption of as-obtained hierarchical nanostructures when In_2O_3 nanoparticles aggregate to larger and uniformly hierarchical nanostructures.[27] In addition, all absorption bands of the as-obtained In_2O_3 nanostructures yielded an onset at around 450 nm, indicating the wide band gap of the as-obtained In_2O_3 nanostructures. These results imply that the UV-vis character of In_2O_3 nanostructures is sensitive to their size and shape.

Supporting Information 13

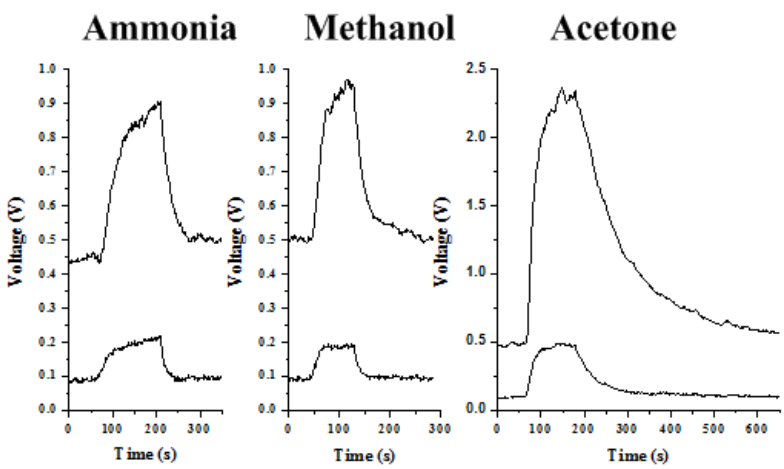

Figure S13. Typical response curves of In_2O_3 hierarchical nanocubes gas sensor (top curve) and In_2O_3 hierarchical nanospheres gas sensor (bottom curve) to different gases with a certain concentration of 400 ppm.

Supporting Information 14

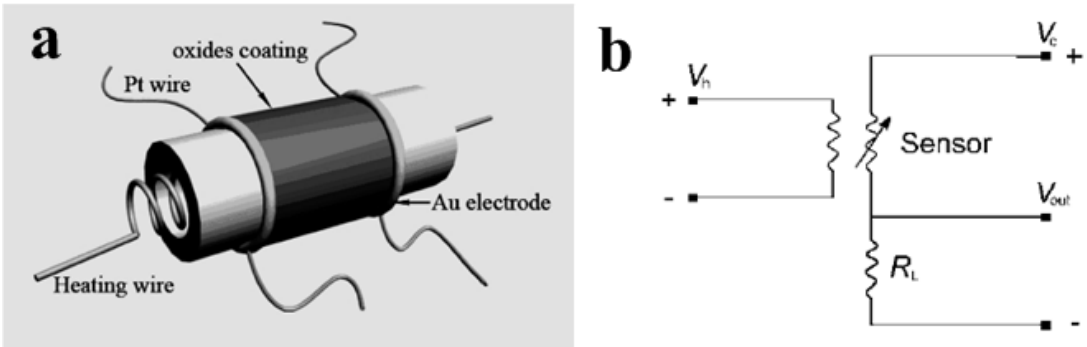

Figure S14. (a) Sketch of the gas sensor and (b) measuring electric circuit of the gas sensor.

Supporting Information 15

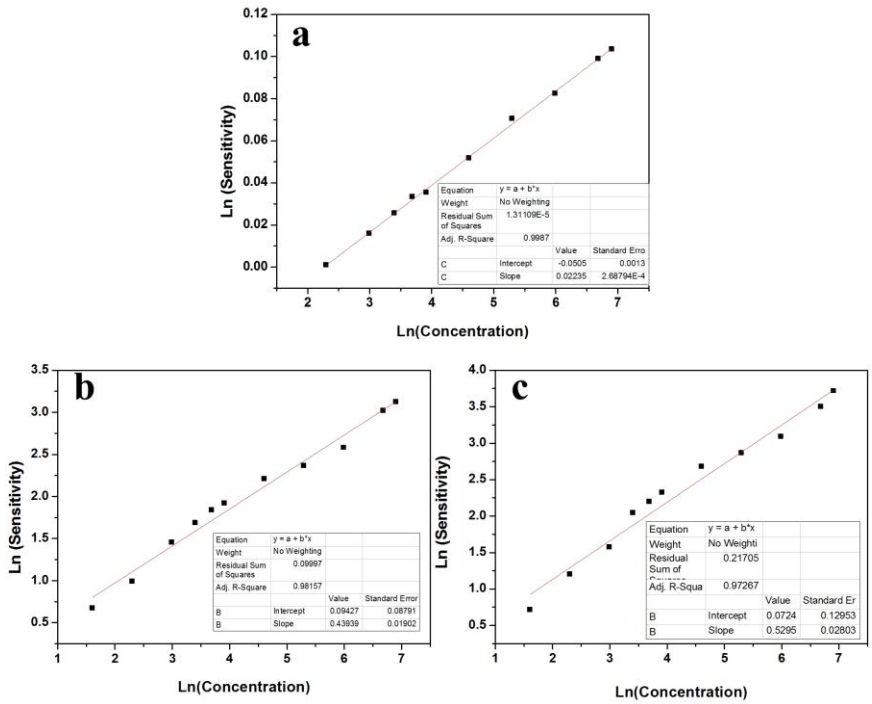

Figure S15. The line relations of ln(sensitivity) to ln (concentration) of (a) In_2O_3 nanoparticle sensors, (b) hierarchical In_2O_3 nanosphere sensors and (c) hierarchical In_2O_3 nanocube sensors.